

An Unconditionally Stable Conformal LOD-FDTD Method for Curved PEC Objects and Its Application to EMC Problems

Hanhong Liu, *Graduate Student Member, IEEE*, Xiaoying Zhao, Xiang-Hua Wang, Shunchuan Yang, *Member, IEEE*, and Zhizhang (David) Chen, *Fellow, IEEE*

Abstract—The traditional finite-difference time-domain (FDTD) method is constrained by the Courant-Friedrich-Levy (CFL) condition and suffers from the notorious staircase error in electromagnetic simulations. This paper proposes a three-dimensional conformal locally-one-dimensional FDTD (CLOD-FDTD) method to address the two issues for modeling perfectly electrical conducting (PEC) objects. By considering the partially filled cells, the proposed CLOD-FDTD method can significantly improve the accuracy compared with the traditional LOD-FDTD method and the FDTD method. At the same time, the proposed method preserves unconditional stability, which is analyzed and numerically validated using the Von-Neuman method. Significant gains in Central Processing Unit (CPU) time are achieved by using large time steps without sacrificing accuracy. Two numerical examples include a PEC cylinder and a missile are used to verify its accuracy and efficiency with different meshes and time steps. It can be found from these examples, the CLOD-FDTD method show better accuracy and can improve the efficiency compared with those of the traditional FDTD method and the traditional LOD-FDTD method.

Index Terms—conformal, EMC problems, FDTD, LOD-FDTD, unconditionally stable.

I. INTRODUCTION

THE finite-difference time-domain (FDTD) method has been widely applied in electromagnetic simulations for its generality and simplicity [1]–[3]. However, it mainly suffers from two issues: one is that time steps are restricted by the Courant-Friedrich-Levy (CFL) condition, which requires prohibitively long simulation time if geometrically fine structures are involved. The other is staircase error since orthogonal hexagonal elements are used to model irregular objects with curved surfaces.

Manuscript received xxx; revised xxx.

This work was supported in part by the National Natural Science Foundation of China through Grant 61801010 and Grant 62071125, in part by Pre-Research Project through Grant J2019-VIII-0009-0170, and Fundamental Research Funds for the Central Universities. (*Corresponding author: Shunchuan Yang*)

H. H. Liu and X. Y. Zhao are with the School of Electronic and Information Engineering of Electronic and Information Engineering, Beihang University, Beijing, China (e-mail: liu759753745@buaa.edu.cn, xyz@buaa.edu.cn).

X. H. Wang is with School of Science, Tianjin University of Technology and Education, Tianjin, China (e-mail: xhwang199@outlook.com).

S. C. Yang is with Research Institute for Frontier Science and School of Electronic and Information Engineering, Beihang University, Beijing, China (e-mail: scyang@buaa.edu.cn).

Z. D. Chen is currently with the College of Physics and Information Engineering, Fuzhou University, Fuzhou, Fujian, P. R. China, on leave from the Department of Electrical and Computer Engineering, Dalhousie University, Halifax, Nova Scotia, Canada B3H 4R2 (email: zz.chen@ieec.org).

To address the first issue, many unconditionally stable FDTD methods, such as the alternately-direction-implicit finite-difference time-domain (ADI-FDTD) method [4] [5], the locally-one-dimensional FDTD (LOD-FDTD) method [6]–[8], the Crank-Nicolson FDTD (CN-FDTD) method [9]–[11], the split-step FDTD (SS-FDTD) method [12]–[14], the leapfrog ADI-FDTD methods [15]–[17] and others, were proposed to remove this constraint, where time steps are independent of mesh sizes. Therefore, stable numerical results can be obtained no matter how large time steps are used in the simulations.

To address the staircase issue, various conformal techniques were proposed to improve the accuracy of the traditional FDTD methods. Then, those conformal techniques were extended for the unconditionally stable FDTD methods, and they can be divided into two groups: one for dielectric media and the other for perfectly electrical conducting (PEC) objects. In [18] [19], area- and volume-weighted techniques were used to calculate the effective permittivity of partially filled cells in the traditional FDTD method. In [20], the conformal techniques were further extended into the high-order FDTD (2,4) method to handle curved dielectric objects. All these techniques show significant accuracy and efficiency improvement compared with the traditional FDTD method. Since only averaged effective parameters are used, their stability can be guaranteed. However, for the curved PEC objects, it is quite challenging. Although these conformal techniques can indeed improve the accuracy, so-called late-time instability occurs if no special treatments are made upon small filled cells [21] [22]. Reduction of time steps is usually required to guarantee stability, which would inevitably increase the cost of Central Processing Unit (CPU) time in practical simulations. Several efforts were made to develop the conformal techniques without reduction of time steps, such as the uniformly-stable-conformal (USC) approach in [23] and the extended cell technique in [24]. However, they are usually complex to implement for practical structures.

To reduce the staircase error in the unconditionally stable FDTD methods, one idea is to extend the conformal techniques employed in the traditional FDTD methods to the implicit FDTD methods to improve the accuracy and keep the unconditional stability. Some efforts, such as the approaches proposed in [25] [26], have been made for this purpose. However, careful investigations show that they are only conditionally stable and suffer from the late-time instability issue. Recently, a two-dimensional conformal LOD-FDTD method was proposed in

[27] to solve the scattering problems.

In this paper, a three-dimensional conformal LOD-FDTD (CLOD-FDTD) method with preserving the unconditional stability for curved PEC objects is proposed to reduce staircase errors. By carefully incorporating partially filled cells into the time-marching formulations, curved surfaces can be accurately modeled through the proposed CLOD-FDTD method. In addition, we numerically proved its stability through the Von-Neuman method with different CFL numbers (CFLNs) and cell sizes. One obvious advantage of the proposed CLOD-FDTD method is that it can improve the accuracy compared with the traditional FDTD method and the LOD-FDTD method and preserve unconditional stability. Therefore, it is much preferred in practical engineering simulations. In [28], we have reported the primary idea about the CLOD-FDTD method. This paper significantly extends our previous work.

The remaining paper is organized as follows. In Section II, a detailed derivation of the proposed CLOD-FDTD method is presented. In Section III, its stability is numerically proved and validated through the Von-Neuman method. For the comparison purpose, the stability of the conformal FDTD method is also included. Then, two numerical examples are carried out to verify its effectiveness in Section IV. At last, we draw some conclusions in Section V.

II. FORMULATIONS FOR THE CLOD-FDTD METHOD

Without loss of generality, a PEC object hosted by linear, lossless, isotropic, and homogeneous medium with permittivity ε and permeability μ is considered in our following derivation. The Maxwell's curl equations can be expressed as

$$\nabla \times \mathbf{H} = \varepsilon \frac{\partial \mathbf{E}}{\partial t}, \quad (1a)$$

$$\nabla \times \mathbf{E} = -\mu \frac{\partial \mathbf{H}}{\partial t}. \quad (1b)$$

To numerically solve (1a) and (1b) with the LOD-FDTD method, they are sampled by Yee's grids in the spatial domain. Two sub-steps scheme is used in the time domain [29]. In this way, each time step is split into two sub-steps. By carefully considering the partially filled cells in Fig. 1, the time-marching formulations for the proposed CLOD-FDTD method in sub-step#1 can be expressed as follows.

Sub-step#1:

$$E_x|_{i+\frac{1}{2},j,k}^{n+\frac{1}{2}} = E_x|_{i+\frac{1}{2},j,k}^n + \frac{\Delta t}{2\varepsilon} \delta_y \left(H_z|_{i+\frac{1}{2},j+\frac{1}{2},k}^n + H_z|_{i+\frac{1}{2},j+\frac{1}{2},k}^{n+\frac{1}{2}} \right), \quad (2a)$$

$$E_y|_{i,j+\frac{1}{2},k}^{n+\frac{1}{2}} = E_y|_{i,j+\frac{1}{2},k}^n + \frac{\Delta t}{2\varepsilon} \delta_x \left(H_x|_{i,j+\frac{1}{2},k+\frac{1}{2}}^n + H_x|_{i,j+\frac{1}{2},k+\frac{1}{2}}^{n+\frac{1}{2}} \right), \quad (2b)$$

$$E_z|_{i,j,k+\frac{1}{2}}^{n+\frac{1}{2}} = E_z|_{i,j,k+\frac{1}{2}}^n + \frac{\Delta t}{2\varepsilon} \delta_x \left(H_y|_{i+\frac{1}{2},j,k+\frac{1}{2}}^n + H_y|_{i+\frac{1}{2},j,k+\frac{1}{2}}^{n+\frac{1}{2}} \right), \quad (2c)$$

$$H_x|_{i,j+\frac{1}{2},k+\frac{1}{2}}^{n+\frac{1}{2}} = H_x|_{i,j+\frac{1}{2},k+\frac{1}{2}}^n + \frac{\Delta t \Delta z}{2\mu S_{yz}|_{i,j+\frac{1}{2},k+\frac{1}{2}}} \times \delta_z \left[l_y|_{i,j+\frac{1}{2},k} \times \left(E_y|_{i,j+\frac{1}{2},k}^n + E_y|_{i,j+\frac{1}{2},k}^{n+\frac{1}{2}} \right) \right], \quad (2d)$$

$$H_y|_{i+\frac{1}{2},j,k+\frac{1}{2}}^{n+\frac{1}{2}} = H_y|_{i+\frac{1}{2},j,k+\frac{1}{2}}^n + \frac{\Delta t \Delta x}{2\mu S_{xz}|_{i+\frac{1}{2},j,k+\frac{1}{2}}} \times \delta_x \left[l_z|_{i,j,k+\frac{1}{2}} \times \left(E_z|_{i,j,k+\frac{1}{2}}^n + E_z|_{i,j,k+\frac{1}{2}}^{n+\frac{1}{2}} \right) \right], \quad (2e)$$

$$H_z|_{i+\frac{1}{2},j+\frac{1}{2},k}^{n+\frac{1}{2}} = H_z|_{i+\frac{1}{2},j+\frac{1}{2},k}^n + \frac{\Delta t \Delta y}{2\mu S_{xy}|_{i+\frac{1}{2},j+\frac{1}{2},k}} \times \delta_y \left[l_x|_{i+\frac{1}{2},j,k} \times \left(E_x|_{i+\frac{1}{2},j,k}^n + E_x|_{i+\frac{1}{2},j,k}^{n+\frac{1}{2}} \right) \right], \quad (2f)$$

where $E_x, E_y, E_z, H_x, H_y, H_z$ denote the electric and magnetic field components, and their subscripts i, j, k are the i th, j th, and k th nodes in the x -, y -, z -directions, respectively. The superscript n is the n th time step in simulations and $\delta_x, \delta_y, \delta_z$ denote the differential operators in the x -, y -, and z -directions, respectively. As shown in Fig. 1, when the curved PEC surfaces exist in the computational domain, l_x, l_y, l_z are edge lengths outside the PEC objects in each cell along the x -, y -, and z -directions, respectively. S_{yz}, S_{xz}, S_{xy} denote the areas outside curved PEC surface projected onto the yoz , xoz , and xoy plane, respectively. It should be noted that in the free space, l_x, l_y, l_z are equal to $\Delta x, \Delta y, \Delta z$, and S_{yz}, S_{xz}, S_{xy} are equal to areas of the corresponding Yee's cell, such as $S_{xy} = \Delta x \Delta y$. Therefore, the time-marching formulations of the CLOD-FDTD method are exactly the same as those of the LOD-FDTD method in the free space. l_x, l_y, l_z are zeros to make H_x, H_y, H_z vanish inside the PEC objects.

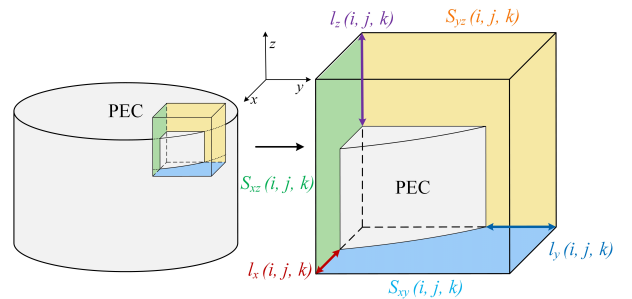


Fig. 1. The view of cells with the curved PEC object projected.

Since the conformal information of partially filled cells is embedded into the time-marching formulations, the curved PEC surface can be considered in the proposed CLOD-FDTD method. Several techniques based on geometrical kernels

[30]–[33] were reported to accurately extract the conformal information for the FDTD method. In our simulations, we also developed a conformal FDTD meshing program based on the ray-tracing algorithm [30] for this purpose. Therefore, the practical engineering structures can be automatically discretized, and the conformal information is accurately extracted.

In a similar manner, the time-marching formulations of the proposed CLOD-FDTD method in sub-step#2 can be expressed as follows.

Sub-step#2:

$$E_x|_{i+\frac{1}{2},j,k}^{n+1} = E_x|_{i+\frac{1}{2},j,k}^{n+\frac{1}{2}} - \frac{\Delta t}{2\varepsilon} \delta_z \left(H_y|_{i+\frac{1}{2},j,k+\frac{1}{2}}^{n+\frac{1}{2}} + H_y|_{i+\frac{1}{2},j,k+\frac{1}{2}}^{n+1} \right), \quad (3a)$$

$$E_y|_{i,j+\frac{1}{2},k}^{n+1} = E_y|_{i,j+\frac{1}{2},k}^{n+\frac{1}{2}} - \frac{\Delta t}{2\varepsilon} \delta_x \left(H_z|_{i+\frac{1}{2},j+\frac{1}{2},k}^{n+\frac{1}{2}} + H_z|_{i+\frac{1}{2},j+\frac{1}{2},k}^{n+1} \right), \quad (3b)$$

$$E_z|_{i,j,k+\frac{1}{2}}^{n+1} = E_z|_{i,j,k+\frac{1}{2}}^{n+\frac{1}{2}} - \frac{\Delta t}{2\varepsilon} \delta_y \left(H_x|_{i,j+\frac{1}{2},k+\frac{1}{2}}^{n+\frac{1}{2}} + H_x|_{i,j+\frac{1}{2},k+\frac{1}{2}}^{n+1} \right), \quad (3c)$$

$$H_x|_{i,j+\frac{1}{2},k+\frac{1}{2}}^{n+1} = H_x|_{i,j+\frac{1}{2},k+\frac{1}{2}}^{n+\frac{1}{2}} - \frac{\Delta t \Delta y}{2\mu S_{yz}|_{i,j+\frac{1}{2},k+\frac{1}{2}}} \times \delta_y \left[l_z|_{i,j,k+\frac{1}{2}} \times \left(E_z|_{i,j,k+\frac{1}{2}}^{n+\frac{1}{2}} + E_z|_{i,j,k+\frac{1}{2}}^{n+1} \right) \right], \quad (3d)$$

$$H_y|_{i+\frac{1}{2},j,k+\frac{1}{2}}^{n+1} = H_y|_{i+\frac{1}{2},j,k+\frac{1}{2}}^{n+\frac{1}{2}} - \frac{\Delta t \Delta z}{2\mu S_{xz}|_{i+\frac{1}{2},j,k+\frac{1}{2}}} \times \delta_z \left[l_x|_{i+\frac{1}{2},j,k} \times \left(E_x|_{i+\frac{1}{2},j,k}^{n+\frac{1}{2}} + E_x|_{i+\frac{1}{2},j,k}^{n+1} \right) \right], \quad (3e)$$

$$H_z|_{i+\frac{1}{2},j+\frac{1}{2},k}^{n+1} = H_z|_{i+\frac{1}{2},j+\frac{1}{2},k}^{n+\frac{1}{2}} - \frac{\Delta t \Delta x}{2\mu S_{xy}|_{i+\frac{1}{2},j+\frac{1}{2},k}} \times \delta_x \left[l_y|_{i,j+\frac{1}{2},k} \times \left(E_y|_{i,j+\frac{1}{2},k}^{n+\frac{1}{2}} + E_y|_{i,j+\frac{1}{2},k}^{n+1} \right) \right]. \quad (3f)$$

Unlike the traditional FDTD method, in which the explicit time-marching formulations are used to update electric and magnetic fields in a leapfrog manner [2], electric fields in the proposed CLOD-FDTD method cannot be explicitly calculated. It requires combining the magnetic and electric field formulations as the LOD-FDTD method. For instance, by

substituting (2f) into (2a), E_x in sub-step#1 can be written as

$$\begin{aligned} & C_1|_{i+\frac{1}{2},j-1,k} E_x|_{i+\frac{1}{2},j-1,k}^{n+\frac{1}{2}} + C_2|_{i+\frac{1}{2},j,k} E_x|_{i+\frac{1}{2},j,k}^{n+\frac{1}{2}} \\ & + C_3|_{i+\frac{1}{2},j+1,k} E_x|_{i+\frac{1}{2},j+1,k}^{n+\frac{1}{2}} \\ & = \frac{\Delta t}{\varepsilon \Delta y} \left(H_z|_{i+\frac{1}{2},j+\frac{1}{2},k}^n - H_z|_{i+\frac{1}{2},j-\frac{1}{2},k}^n \right) \\ & - C_1|_{i+\frac{1}{2},j-1,k} E_x|_{i+\frac{1}{2},j-1,k}^n + C_4|_{i+\frac{1}{2},j,k} E_x|_{i+\frac{1}{2},j,k}^n \\ & - C_3|_{i+\frac{1}{2},j+1,k} E_x|_{i+\frac{1}{2},j+1,k}^n, \end{aligned} \quad (4)$$

where

$$\begin{aligned} C_1|_{i+\frac{1}{2},j-1,k} &= -\frac{\Delta t^2 l_x|_{i+\frac{1}{2},j-1,k}}{4\mu\varepsilon\Delta y S_{xy}|_{i+\frac{1}{2},j-\frac{1}{2},k}}, \\ C_2|_{i+\frac{1}{2},j,k} &= 1 + \frac{\Delta t^2}{4\mu\varepsilon\Delta y} \left(\frac{l_x|_{i+\frac{1}{2},j,k}}{S_{xy}|_{i+\frac{1}{2},j+\frac{1}{2},k}} + \frac{l_x|_{i+\frac{1}{2},j,k}}{S_{xy}|_{i+\frac{1}{2},j-\frac{1}{2},k}} \right), \\ C_3|_{i+\frac{1}{2},j+1,k} &= -\frac{\Delta t^2 l_x|_{i+\frac{1}{2},j+1,k}}{4\mu\varepsilon\Delta y S_{xy}|_{i+\frac{1}{2},j+\frac{1}{2},k}}, \\ C_4|_{i+\frac{1}{2},j,k} &= 1 - \frac{\Delta t^2}{4\mu\varepsilon\Delta y} \left(\frac{l_x|_{i+\frac{1}{2},j,k}}{S_{xy}|_{i+\frac{1}{2},j+\frac{1}{2},k}} + \frac{l_x|_{i+\frac{1}{2},j,k}}{S_{xy}|_{i+\frac{1}{2},j-\frac{1}{2},k}} \right). \end{aligned}$$

Similarly, by substituting (3f) into (3a), E_x in sub-step#2 can be expressed as

$$\begin{aligned} & C_5|_{i+\frac{1}{2},j,k-1} E_x|_{i+\frac{1}{2},j,k-1}^{n+1} + C_6|_{i+\frac{1}{2},j,k} E_x|_{i+\frac{1}{2},j,k}^{n+1} \\ & + C_7|_{i+\frac{1}{2},j,k+1} E_x|_{i+\frac{1}{2},j,k+1}^{n+1} \\ & = -\frac{\Delta t}{\varepsilon \Delta z} \left(H_y|_{i+\frac{1}{2},j,k+\frac{1}{2}}^{n+\frac{1}{2}} - H_y|_{i+\frac{1}{2},j,k-\frac{1}{2}}^{n+\frac{1}{2}} \right) \\ & - C_5|_{i+\frac{1}{2},j,k-1} E_x|_{i+\frac{1}{2},j,k-1}^{n+\frac{1}{2}} + C_8|_{i+\frac{1}{2},j,k} E_x|_{i+\frac{1}{2},j,k}^{n+\frac{1}{2}} \\ & - C_7|_{i+\frac{1}{2},j,k+1} E_x|_{i+\frac{1}{2},j,k+1}^{n+\frac{1}{2}}, \end{aligned} \quad (5)$$

where

$$\begin{aligned} C_5|_{i+\frac{1}{2},j,k-1} &= -\frac{\Delta t^2 l_x|_{i+\frac{1}{2},j,k-1}}{4\mu\varepsilon\Delta z S_{xz}|_{i+\frac{1}{2},j,k-\frac{1}{2}}}, \\ C_6|_{i+\frac{1}{2},j,k} &= 1 + \frac{\Delta t^2}{4\mu\varepsilon\Delta z} \left(\frac{l_x|_{i+\frac{1}{2},j,k}}{S_{xz}|_{i+\frac{1}{2},j,k+\frac{1}{2}}} + \frac{l_x|_{i+\frac{1}{2},j,k}}{S_{xz}|_{i+\frac{1}{2},j,k-\frac{1}{2}}} \right), \\ C_7|_{i+\frac{1}{2},j,k+1} &= -\frac{\Delta t^2 l_x|_{i+\frac{1}{2},j,k+1}}{4\mu\varepsilon\Delta z S_{xz}|_{i+\frac{1}{2},j,k+\frac{1}{2}}}, \\ C_8|_{i+\frac{1}{2},j,k} &= 1 - \frac{\Delta t^2}{4\mu\varepsilon\Delta z} \left(\frac{l_x|_{i+\frac{1}{2},j,k}}{S_{xz}|_{i+\frac{1}{2},j,k+\frac{1}{2}}} + \frac{l_x|_{i+\frac{1}{2},j,k}}{S_{xz}|_{i+\frac{1}{2},j,k-\frac{1}{2}}} \right). \end{aligned}$$

It can be found that (4) and (5) are similar to the traditional LOD-FDTD time-marching formulations while $C_1 - C_8$ are modified by S_{yz}, S_{xz}, S_{xy} and l_x, l_y, l_z through carefully considering partially filled cells near the curved PEC surfaces. It is necessary to collect all the electric field components into the compact matrix equation form for solving their field values.

By rewriting the time-marching formulation (4) into the matrix form, we obtain

$$\mathbf{A}\mathbf{E}_x^{n+\frac{1}{2}} = \mathbf{r}^n, \quad (6)$$

where the square coefficient matrix \mathbf{A} with the dimension of $N \times N$, where N is the total number of E_x nodes along the y -direction, is tridiagonal, and the column vector \mathbf{r}^n contains all values on the right-hand side of (4) in a column-wise fashion. (6) can be efficiently solved by the Thomas Algorithm [34]. E_y and E_z can be also easily calculated in a similar manner. Once all the electric fields are calculated, the magnetic fields can be explicitly updated through (2d)-(2f) and (3d)-(3f).

III. STABILITY ANALYSIS OF THE PROPOSED CLOD-FDTD METHOD AND THE CONFORMAL FDTD METHOD

In this section, the Von-Neuman method [35] is used to prove the stability of the proposed CLOD-FDTD method and the conformal FDTD (CFDTD) method, which transforms electromagnetic field components in the time domain into time-harmonic counterparts, and then analyze the eigenvalues of the coefficient matrix. If the modulus of all eigenvalues are not larger than one, the proposed CLOD method is unconditionally stable.

For the time-harmonic fields, we have the following relationship

$$\mathbf{U}^{n+1} = e^{j\omega\Delta t}\mathbf{U}^n, \quad (7)$$

where \mathbf{U}^n and \mathbf{U}^{n+1} denote column vectors of electromagnetic fields at the n th and $n + 1$ th time step. For the Von-Neuman method, we have $\mathbf{U}^n = [E_x^n, E_y^n, E_z^n, H_x^n, H_y^n, H_z^n]^T$, where $E_x^n, E_y^n, E_z^n, H_x^n, H_y^n, H_z^n$ are field values in the spectral domain.

A. Stability Analysis of the Proposed CLOD-FDTD Method

To make our derivation clear, we define a column vector $\mathbf{U} = [E_x^n, E_y^n, E_z^n, H_x^n, H_y^n, H_z^n]^T$, where $E_x^n, E_y^n, E_z^n, H_x^n, H_y^n$, and H_z^n include all the corresponding field nodes on Yee's grid in the x -, y -, z -directions, respectively. Take E_x^n as an example, $E_x^n = [E_x|_{1,1,1}^n, E_x|_{2,1,1}^n, \dots, E_x|_{m,p+1,q+1}^n]^T$, where the subscripts m , p , and q denote field components' indices in x -, y - and z -directions, respectively.

According to (4), the amplification matrix $\mathbf{\Lambda}_1$ for sub-step#1 is given by

$$\mathbf{U}^{n+\frac{1}{2}} = \mathbf{\Lambda}_1\mathbf{U}^n. \quad (8)$$

Similarly, the amplification matrix $\mathbf{\Lambda}_2$ for sub-step#2 can be obtained as

$$\mathbf{U}^{n+1} = \mathbf{\Lambda}_2\mathbf{U}^{n+\frac{1}{2}}. \quad (9)$$

By substituting (8) into (9), we obtain the following matrix equation

$$\mathbf{U}^{n+1} = \mathbf{\Lambda}\mathbf{U}^n. \quad (10)$$

If the modulus of all eigenvalues in $\mathbf{\Lambda}$ are less than or equal to one, the proposed CLOD-FDTD method is stable. When the homogeneous medium and uniform cells are used, the dimension of $\mathbf{\Lambda}$ can be reduced to 6×6 . Its 6 eigenvalues

can be analytically calculated, and then compared with one. However, the scenario for the proposed CLOD-FDTD methods is different since S_{yz}, S_{xz}, S_{xy} and l_x, l_y, l_z are location-dependent. It cannot be dealt with the mentioned approaches in [5] [17]. To address this issue, we use a specific example to demonstrate the stability of the proposed CLOD-FDTD method.

Fig. 2 shows the geometrical configuration to validate the numerical stability. A cubic cavity filled with air is considered, and its boundaries are the perfect electric conductor. The size of the cavity is $2m \times 2m \times 2m$. A PEC cylinder is placed at the middle of the cavity, and its diameter and height are both $1m$.

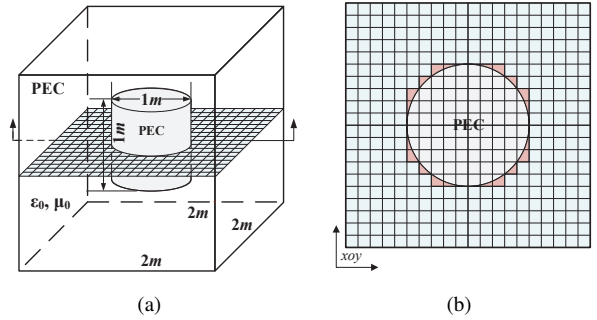


Fig. 2. (a) The geometrical configuration of the PEC cylinder and the PEC cavity, (b) the Yee's grid with cell size $0.1m$ at $z = 1m$.

Three grids with cell sizes $0.25m$, $0.125m$, and $0.1m$ are used to discretize the structures, and a horizontal view of Yee's grid with cell size $0.1m$ at $z = 1m$ is shown in Fig. 2(b). It is easy to find that many partially filled cells, which are marked in light red, exist. Once the conformal meshes are generated, the coefficients in (4)-(5) can be calculated, and then all the eigenvalues of $\mathbf{\Lambda}$ can be numerically computed through the Matlab command "eig(·)".

Figs. 3-5 show the eigenvalues of $\mathbf{\Lambda}$ for the proposed CLOD-FDTD method with different CFLNs. CFLN is the ratio of time step Δt used in the simulation to the maximum time step Δt_{\max} defined by the CFL condition. Δt_{\max} is given by

$$\Delta t_{\max} = \frac{1}{c\sqrt{(\Delta x)^{-2} + (\Delta y)^{-2} + (\Delta z)^{-2}}}, \quad (11)$$

where c denotes the electromagnetic wave velocity in the air. In each grid size, four scenarios with CFLN = 1, 4, 8 and 64 are shown in this paper. It can be found that all the eigenvalues fall on the unit circle in Figs. 3-5. Although only twelve specific scenarios are presented in this subsection, we have done a number of numerical verification to cover the general situations in the practical simulations. Without exception, all the eigenvalues of $\mathbf{\Lambda}$ fall on the unit circle. Therefore, we can safely draw the conclusion that the proposed conformal LOD-FDTD method is unconditionally stable.

B. Stability Analysis of the CFDTD Method

For comparison purposes, we further analyze the stability of the traditional CFDTD method based on [36] in a similar

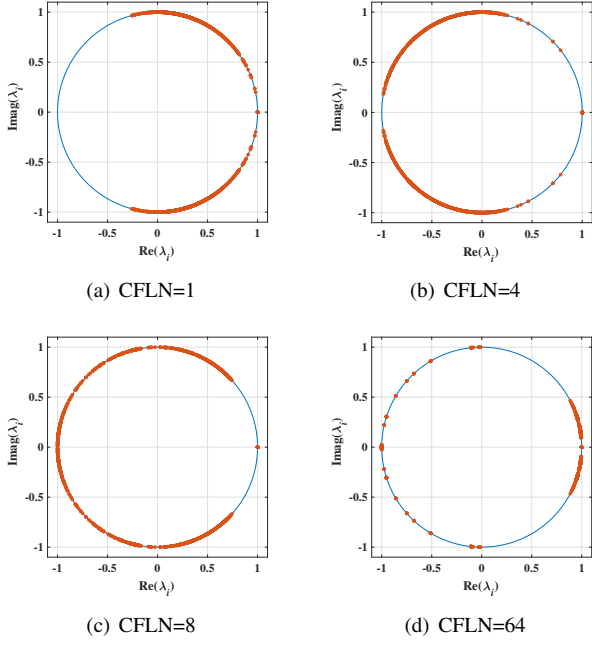


Fig. 3. The eigenvalues of Λ for the proposed CLOD-FDTD method with mesh size $0.25m$ for CFLN = 1, 4, 8, and 64, respectively.

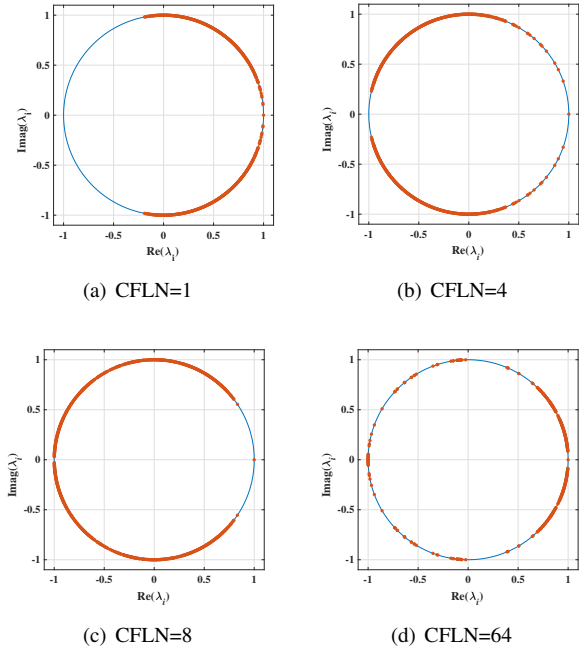


Fig. 4. The eigenvalues of Λ for the proposed CLOD-FDTD method with mesh size $0.125m$ for CFLN = 1, 4, 8, and 64, respectively.

manner. By taking E_x, H_z as examples, the time-marching formulations of the CFDTD method can be expressed as

$$\begin{aligned}
 E_x|_{i+\frac{1}{2},j,k}^{n+1} &= E_x|_{i+\frac{1}{2},j,k}^n \\
 &+ \frac{\Delta t}{\varepsilon \Delta y} \left(H_z|_{i+\frac{1}{2},j+\frac{1}{2},k}^{n-\frac{1}{2}} - H_z|_{i+\frac{1}{2},j-\frac{1}{2},k}^{n-\frac{1}{2}} \right) \\
 &- \frac{\Delta t}{\varepsilon \Delta z} \left(H_y|_{i+\frac{1}{2},j,k+\frac{1}{2}}^{n-\frac{1}{2}} - H_y|_{i+\frac{1}{2},j,k-\frac{1}{2}}^{n-\frac{1}{2}} \right), \quad (12a)
 \end{aligned}$$

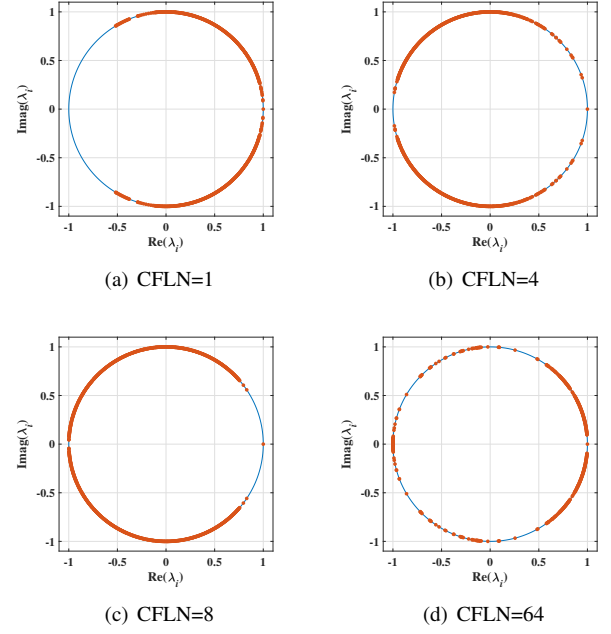


Fig. 5. The eigenvalues of Λ for the proposed CLOD-FDTD method with mesh size $0.1m$ for CFLN = 1, 4, 8, and 64, respectively.

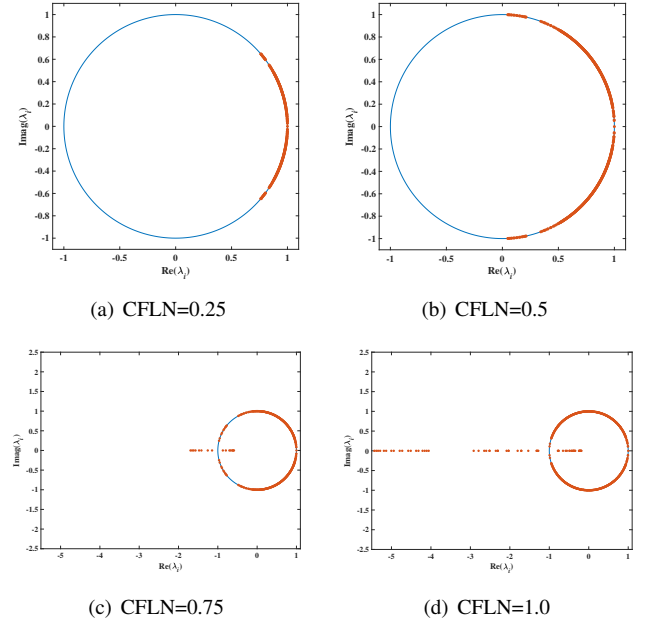


Fig. 6. The eigenvalues of Λ in the CFDTD method with CFLN = 0.25, 0.5, 0.75 and 1.0, respectively.

$$\begin{aligned}
 H_z|_{i+\frac{1}{2},j+\frac{1}{2},k}^{n+\frac{1}{2}} &= H_z|_{i+\frac{1}{2},j+\frac{1}{2},k}^{n-\frac{1}{2}} \\
 &+ \frac{\Delta t \Delta y}{\mu S_{xy}|_{i+\frac{1}{2},j+\frac{1}{2},k}} \delta y \left(l_x|_{i+\frac{1}{2},j,k} E_x|_{i+\frac{1}{2},j,k}^n \right) \\
 &- \frac{\Delta t \Delta x}{\mu S_{xy}|_{i+\frac{1}{2},j+\frac{1}{2},k}} \delta x \left(l_y|_{i,j+\frac{1}{2},k} E_y|_{i,j+\frac{1}{2},k}^n \right), \quad (12b)
 \end{aligned}$$

where δ_x, δ_y denote the differential operators in the x - and y -directions, respectively, and l_x, l_y, S_{xy} are conformal coefficients, which are exactly the same as those in the proposed

CLOD-FDTD method. It should be noted that the electric and magnetic components in the CFDTD method are assigned at different time instances. By using (7), \mathbf{U}^n for the CFDTD method is slightly modified as

$$\mathbf{U}^n = \left[\mathbf{E}_x^n, \mathbf{E}_y^n, \mathbf{E}_z^n, \mathbf{H}_x^{n-\frac{1}{2}}, \mathbf{H}_y^{n-\frac{1}{2}}, \mathbf{H}_z^{n-\frac{1}{2}} \right]^T. \quad (13)$$

The amplification matrix $\mathbf{\Lambda}_{\text{CFDTD}}$ of the CFDTD method can be obtained as

$$\mathbf{U}^{n+1} = \mathbf{\Lambda}_{\text{CFDTD}} \mathbf{U}^n. \quad (14)$$

The structure in Fig. 2 is still used to illustrate the stability. Yee's grids with the mesh size of $0.125m$ are used to discretize the structure. All eigenvalues with CFLN = 0.25, 0.5, 0.75, and 1.0 are shown in Fig. 6(a)-(d).

It can be found that from Figs. 6(a) and (b), the eigenvalues fall on the unit circle. Therefore, the CFDTD is stable when CFLN is less than 0.5 with the mesh size being $0.125m$. However, some eigenvalues fall outside the unit circle in Figs. 6(c) and (d), which implies that the CFDTD method is unstable if the time step increases to 0.75 times of Δt_{max} . The stability of the CFDTD method strongly depends on S_{yz}, S_{xz}, S_{xy} and l_x, l_y, l_z . The CFLNs must be decreased as the ratio $l_{\text{max}}/S_{\text{min}}$ decrease. Therefore, when the finer meshes are used, the CFLNs should be smaller. To obtain stable numerical results, quite small time steps may be required, which is undesirable in practical simulations. In addition, if the CFDTD is unstable, the maximum modulus value of the eigenvalues also increases as CFLN increases, which makes the CFDTD solution divergent faster as time steps increase.

C. Numerical Verification

To further illustrate the stability of the proposed CLOD-FDTD method and the CFDTD method, a series of numerical simulations are performed with different CFLNs. In these simulations, the grids with cell size of $0.05m$ are used to discretize a cubic cavity with a PEC cylinder, as shown in Fig. 2. The overall simulation time is $36\mu\text{s}$ when CFLN = 1, 4, 8, and 64. A line differentiated Gaussian pulse current source along the z-direction, as shown in Fig. 7, is located at $(0.5, 0.5, 1.0)[m]$, and an observation point is located at $(0.5, 1.5, 1.0)[m]$.

Fig. 8(a)-(d) show E_z verse time with CFLN = 1, 4, 8, and 64, respectively. The overall time steps are 373,864, 93,466, 46,733, and 5,841 when CFLN = 1, 4, 8 and 64, respectively. It can be found that all the simulations are stable even if quite large time steps are used, which confirms our conclusion through the eigenvalue analysis.

In addition, it can be found that the results obtained by the CLOD-FDTD method show some difference when different CFLNs are used. The reason is that the dispersion error is diverse for different CFLNs [37]–[39]. According to [40], as CFLNs increase, the dispersion error in the LOD-FDTD method also increases. Therefore, results obtained with CFLN = 64 have large error comparing with other situations. Since the long time step with CFLN = 64 will cause serious impact on stability, we choose this CFLN to prove the strong stability of the proposed CLOD-FDTD method.

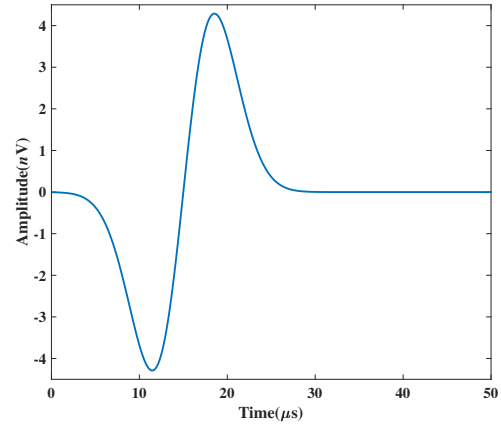


Fig. 7. The differentiated Gaussian pulse used as the excitation.

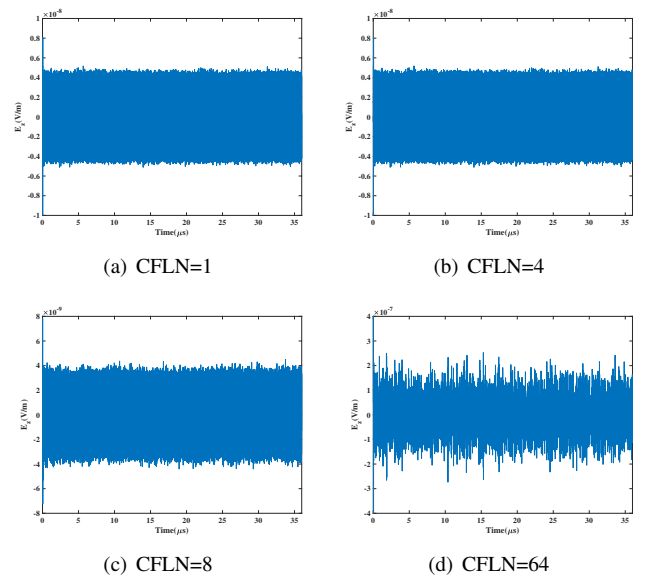


Fig. 8. The E_z field values verse time steps with CFLN = 1, 4, 8 and 64, respectively.

We performed another numerical simulation for comparison, where the CFDTD method with CFLN = 0.51 and the CLOD-FDTD method with CFLN = 1 are used. The overall time is $1.8\mu\text{s}$, which requires 36,975 time steps to complete this simulation in the CFDTD method and 18,693 time steps in the proposed CLOD-FDTD method. To make the comparison fair for the CLOD-FDTD method and the CFDTD method, the same grids with cell size $0.05m$ are used. Fig. 9 shows results obtained from the CFDTD method and the proposed CLOD-FDTD method. It is easy to find that from $0\mu\text{s}$ to $0.18\mu\text{s}$, results obtained from the two methods agree well with each other. However, results obtained from the CFDTD method gradually divergent, and the simulation becomes unstable in the end. For the proposed CLOD-FDTD method, the simulation is always stable with no sign of instability, which confirms our previous analysis.

Here we only present some numerical results for a specific example. In addition, we carried out a number of numerical

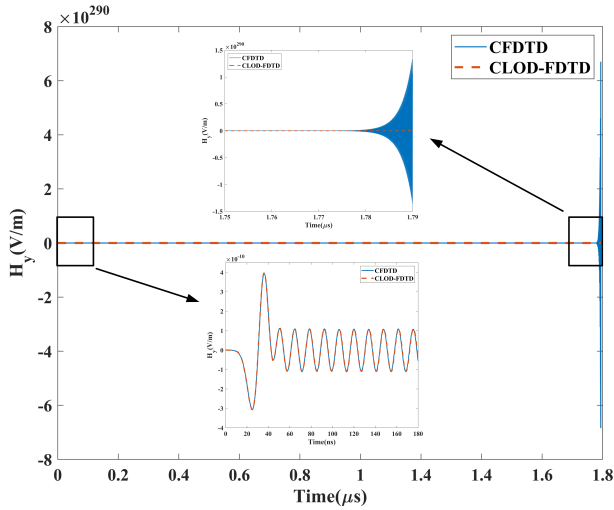


Fig. 9. The E_z field values verse time step obtained from the proposed LOD-FDTD method with CFLN = 1 and the CFDTD method with CFLN = 0.51.

simulations and eigenvalue analyses, which confirm our analysis. In summary, all the analyses mentioned above show that the conformal LOD-FDTD method is unconditionally stable for curved PEC objects.

IV. NUMERICAL RESULTS AND DISCUSSION

In this section, two numerical examples are carried out to validate the accuracy and efficiency of the proposed CLOD-FDTD method. Results computed by the FDTD method and the LOD-FDTD method are also provided for comparison. All the in-house codes are written using C++ and linked in the release mode with exactly the same configurations. They are run on a workstation including an Intel Gold 6143 CPU with the operating frequency of 3.2 GHz and 256 GB memory. For a fair comparison, all codes are run in a single thread.

A. A PEC Cylinder Object in A Cavity

In this subsection, a PEC cylinder is considered to validate the accuracy of the proposed CLOD-FDTD method, as shown in the previous section. Its diameter and height are $1m$. It is placed at the center of a PEC cubic cavity. The PEC cavity is filled with air, and its dimension is $2m \times 2m \times 2m$. The top-down and front-back views of this structure are shown in Figs. 10(a) and (b), respectively.

Two uniform meshes with cell sizes $0.05m$ and $0.01m$ are used to discretize the structure. Coarse meshes with cell size $0.05m$ are used in the proposed CLOD-FDTD method, and both the coarse and fine meshes are used in the LOD-FDTD method and the FDTD method.

A line differential Gaussian pulse current source $f = (t - t_0)e^{[-(t-t_0)^2/\tau^2]}$ with $t_0 = 3\tau$, $\tau = 10ns$ is used as an excitation function. Its location is $(0.5, 0.5, 1.0)[m]$ in both coarse and fine meshes. The observation point is located at $(1.5, 1.5, 1.0)[m]$. The overall physical time is $2.4\mu s$.

The normalized frequency responses of H_y are shown in Fig. 11 with CFLN = 1 for three methods. It can be found

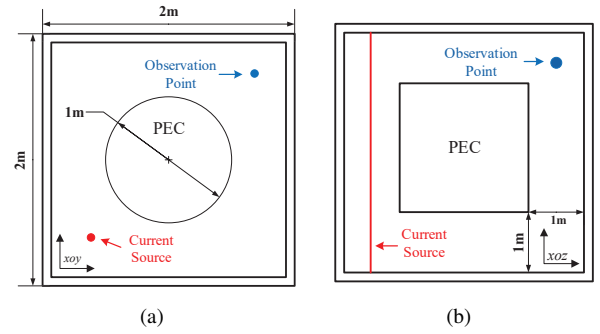


Fig. 10. The top-down and front-back views of the structure: (a) the top-down view, (b) the front-back view.

that results obtained from the LOD-FDTD method and the FDTD method show good agreement with both coarse and fine meshes. Therefore, when time steps and meshes used in the simulations are the same, the LOD-FDTD method and the FDTD method can achieve a similar level of accuracy. However, when coarse meshes with cell size $0.05m$ are used in the proposed CLOD-FDTD method, its frequency response shows excellent agreement with those from the LOD-FDTD method and FDTD method with fine meshes of cell size $0.01m$. Therefore, significant accuracy improvement can be achieved for the proposed CLOD-FDTD method. It should be noted that the time step used in the proposed CLOD-FDTD method is five times those for the other two methods since the cell size of coarse meshes ($0.05m$) is five times as that of fine meshes ($0.01m$). In order to compare the accuracy of various FDTD methods, the resonant frequency obtained by the HFSS based on the FEM is included, as shown in Fig. 11.

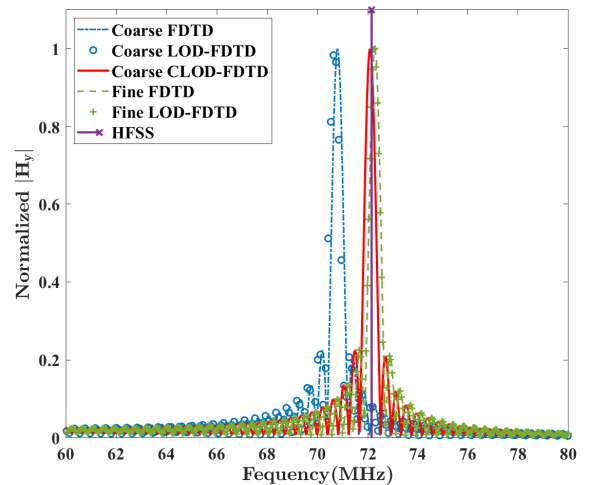


Fig. 11. The normalized frequency responses of H_y obtained from the FDTD method, the LOD-FDTD method, the proposed CLOD-FDTD method with CFLN = 1 and different mesh sizes, and the HFSS for the PEC cavity

Since the proposed CLOD-FDTD method is unconditionally stable, CPU time can be further reduced as CFLN increases. Fig. 12 shows the normalized frequency responses obtained from the CLOD-FDTD method with CFLN = 1 and 4. Mesh size $0.05m$ is used in the proposed CLOD-FDTD method. The

reference results are obtained from the LOD-FDTD method with coarse meshes when CFLN = 1, 4, and the LOD-FDTD method with fine meshes when CFLN = 1.

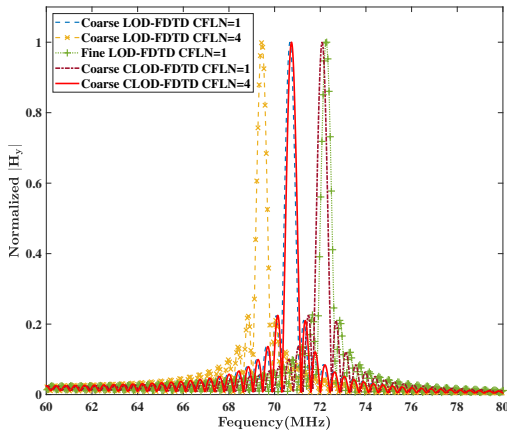


Fig. 12. The normalized frequency responses of H_y obtained from the LOD-FDTD method and the CLOD-FDTD method with CFLN = 1 and 4.

As shown in Fig. 12, results obtained from the CLOD-FDTD method with CFLN = 1 agree well with those obtained from the LOD-FDTD method with fine meshes of cell size $0.01m$ and CFLN = 1. When CFLN = 1 and coarse meshes are used, the resonant frequency obtained from the LOD-FDTD method shows large discrepancy with the reference solutions. Furthermore, when CFLN = 4 and coarse meshes are used, results obtained from the LOD-FDTD method show even larger errors. Since the dispersion error in the LOD-FDTD method with CFLN = 4 is larger than that of the LOD-FDTD method with CFLN = 1, results in Fig. 11 are different from each other. However, when the proposed CLOD-FDTD method with CFLN = 4 is used to complete this simulation, and coarse meshes are used, its results show good agreement with those obtained from the LOD-FDTD method with CFLN = 1. Therefore, the efficiency of the proposed CLOD-FDTD method can be further improved compared with the conventional LOD-FDTD method.

Moreover, some comparisons between the LOD-FDTD method and the CLOD-FDTD method in the time domain, as shown in Fig. 13. The sizes of fine and coarse meshes are $0.01m$, $0.05m$, respectively. From Fig. 13, it can be found that the amplitudes of waveforms obtained with CFLN = 8 are larger than those with CFLN = 1. Furthermore, differences between results with CFLN = 8 and CFLN = 1 become larger as the simulation goes by. However, results obtained by the CLOD-FDTD method still have higher accuracy than that of the LOD-FDTD method.

The total time cost to finish the simulations is listed in Table I. The overall time is $180ns$. Mesh sizes are $0.05m$ and $0.01m$ for coarse and fine meshes, respectively. Since the CFDTD method is unstable with CFLN = 0.25 in fine meshes, CFLN is set as 0.1 for fine meshes to guarantee the stability. It can be found that from Table I, the CFDTD method with CFLN = 0.5 is faster than the CLOD-FDTD method with CFLN = 1 when coarse meshes are used. However, as CFLN increases,

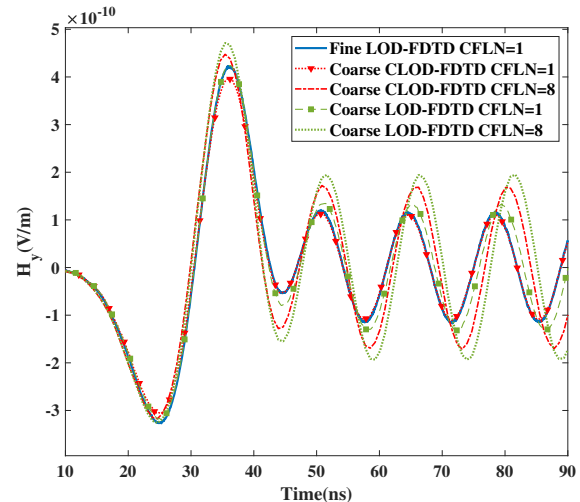


Fig. 13. The responses of H_y obtained from the LOD-FDTD method and the CLOD-FDTD method with CFLN = 1 and 8.

the CLOD-FDTD method gradually outperforms the CFDTD method for two reasons: one is that the CFDTD method has to reduce the CFLN to guarantee the stability, and the other is that the overall count of cells significantly increases in fine meshes.

TABLE I
THE COMPUTATIONAL CONSUMPTION OF THE LOD-FDTD METHOD THE CLOD-FDTD METHOD AND THE CFDTD METHOD WITH CFLN = 1,4 AND DIFFERENT MESHES

Method		CFLN	Δt [ns]	No. of Cells	Time Cost [s]	Ratio*
LOD-FDTD	Coarse	1	0.092	64,000	14.2	1107.3
		4	0.385	64,000	3.6	4367.7
	Fine	1	0.019	8,000,000	15723.7	1.0
		4	0.073	8,000,000	4253.5	3.7
CLOD-FDTD	Coarse	1	0.092	64,000	22.6	695.7
	4	0.385	64,000	5.5	2858.9	
CFDTD	Coarse	0.5	0.048	64,000	7.2	2183.8
	Fine	0.1	0.0019	8,000,000	21978.9	0.71

* Ratio is defined as the ratio of time cost used in the LOD-FDTD method with fine meshes to that of the corresponding method.

In summary, the proposed CLOD-FDTD method shows better accuracy compared with the FDTD method and the LOD-FDTD method, when the same meshes and time step are used. Significant accuracy improvement of the proposed CLOD-FDTD method is obtained compared with the LOD-FDTD method, when the same meshes are used. Therefore, we can obtain accurate results with relative coarse meshes and large time steps without compromising the accuracy. Consequently, CPU time can be saved in simulations.

B. The Electromagnetic Scattering from A Missile

In this section, a PEC missile, which is $10.2m$ long, $6.55m$ wide, and $2.55m$ high, is considered. The convolution perfectly matched layer (CPML) based on [41] [42] is used to truncate the computational domain. The geometrical model is shown in Fig. 14. Its surrounding medium is the vacuum.

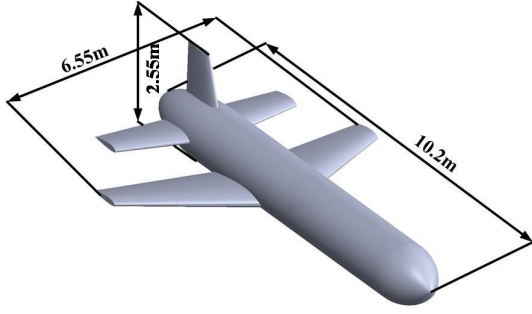


Fig. 14. The geometrical model of the missile.

The grids with mesh sizes $0.1m$ and $0.025m$ are used to discretize the missile. Coarse meshes are used in the CLOD-FDTD method, and both the coarse and fine meshes are used in the conventional LOD-FDTD method and the FDTD method for the references.

Fig. 15 shows Yee’s grids and the conformal grids when mesh size is $0.1m$. The normal Yee’s grids are used in the traditional FDTD method and the LOD-FDTD method, while the conformal grids are used in the CLOD-FDTD method. In Yee’s grids, large geometrical modeling error occurs due to the rectangular cells. However, the conformal grids fit well with the original model. For example, the curved structures of the missile, such as wings and the missile head, are accurately modeled through the conformal grids, as shown in Fig. 15 (b).

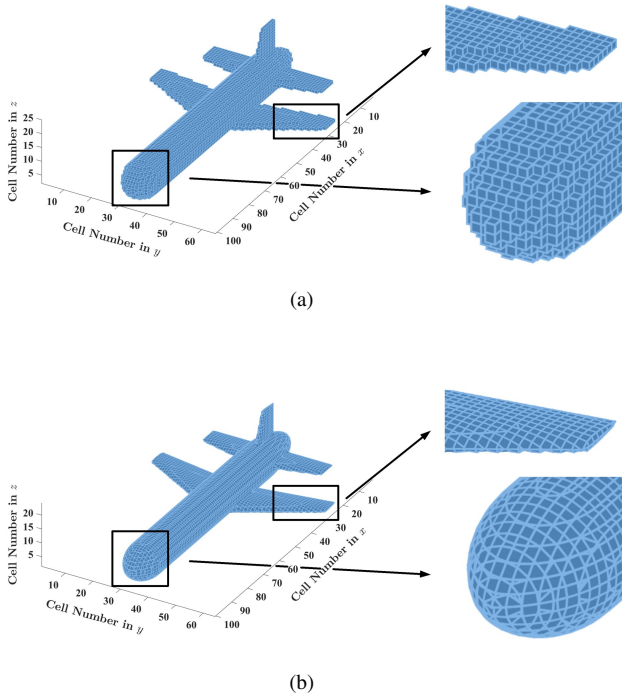


Fig. 15. The meshes of an ideal conductor missile with mesh size $0.1 m$: (a) Yee’s meshes, (b) the conformal meshes.

A line current source with the differential Gaussian pulse $f = (t-t_0)e^{[-(t-t_0)^2/\tau^2]}$ $t_0 = 3\tau$, $\tau = 10ns$ in the x direction

is used as the excitation function. The current source is located at $(9, 2.5, 1.4)[m]$ in both coarse mesh and fine mesh.

E_x at $66ns$ is recorded when $CFLN = 1$, three slices parallel to the xoy , $yozy$, $xozy$ plane are shown in Fig. 16. Figs. 16(a)-(c) show $\log(|E_x|)$ obtained by the FDTD method, the LOD-FDTD method, and the CLOD-FDTD method with coarse meshes. Figs. 16(d) shows $\log(|E_x|)$ obtained by the LOD-FDTD method with fine meshes. It can be found from Fig. 16(a)-(b) that results obtained by the FDTD and LOD-FDTD methods fit well with each other. However, comparing to Figs. 16(a)-(b), results obtained by the CLOD-FDTD method with coarse meshes have a different distribution of E_x at the tail of the missile and the junction of field slices parallel to xoy and $yozy$ plane. Meanwhile, results obtained by the LOD-FDTD method with fine meshes agree well with results obtained by the CLOD-FDTD method with coarse meshes in the exterior region.

Furthermore, $\log(|E_x|)$ in the CLOD-FDTD method with coarse meshes and the LOD-FDTD method with fine meshes at $30ns$, $60ns$, $90ns$, $120ns$ are shown in Fig. 17 and Fig. 18, relatively. Their results agree well with each other in the exterior region.

It should be noted that the results obtained by the CLOD-FDTD method in Figs. 16-17 has obvious difference with other results in the wings and tail. It is the conformal meshes that modify the magnetic field attached to the PEC surface, which makes E_x near the PEC surface larger than those in the traditional FDTD method and the LOD-FDTD method. In fact, it can be seen from Fig. 15(b), the physical thickness of the wings is smaller than that of Yee’s meshes in Fig. 15(a). It is obvious that electric fields at the meshes which are located at the bottom surface of wings are outside the PEC object. Therefore, those electric fields should not be zeros. However, the traditional FDTD method and the LOD-FDTD method enforce electric fields to be zeros at those positions due to staircase error. Since the conformal meshes in Fig. 15(b) are used in the proposed CLOD-FDTD method and partially filled cells are carefully considered, the error is significantly reduced in the CLOD-FDTD method. Therefore, the CLOD-FDTD method can obtain more accurate results than those from the LOD-FDTD method and the FDTD method with the same meshes.

Moreover, the electric field at the observation point was recorded to validate the effectiveness of the proposed CLOD-FDTD method. The observation point is set at $(9, 3, 1.4)[m]$ in both fine and coarse mesh. The transient values of E_y are shown in Fig. 19. It can be found that results obtained from the LOD-FDTD method, and the FDTD method show good agreement. Simultaneously, it can be found that results obtained from the CLOD-FDTD method with coarse meshes agree well with those from the LOD-FDTD method and the FDTD method with fine meshes. Therefore, the CLOD-FDTD method can obtain accurate results with coarse meshes.

E_y obtained from the CLOD-FDTD method, and the LOD-FDTD method with different $CFLN$ are shown in the Fig. 20. Fine meshes are used in the LOD-FDTD method with $CFLN = 1, 4$. Coarse meshes are used in the CLOD-FDTD method and the LOD-FDTD method with $CFLN = 4$. It can be seen

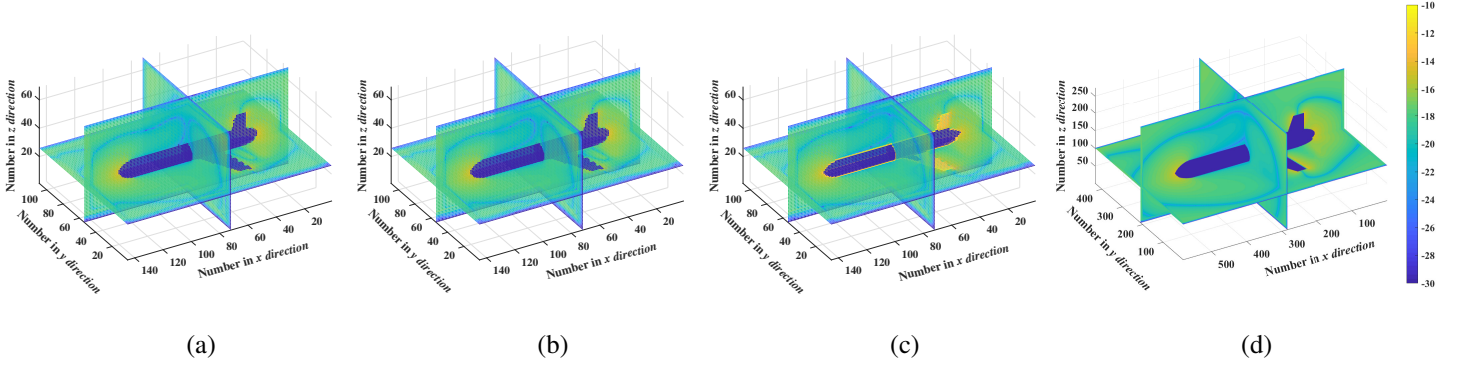


Fig. 16. The $\log(|E_x|)$ at $66ns$: (a) the FDTD method with coarse meshes, (b) the LOD-FDTD method with coarse meshes, (c) the CLOD-FDTD method with coarse meshes, (d) the LOD-FDTD method with fine meshes.

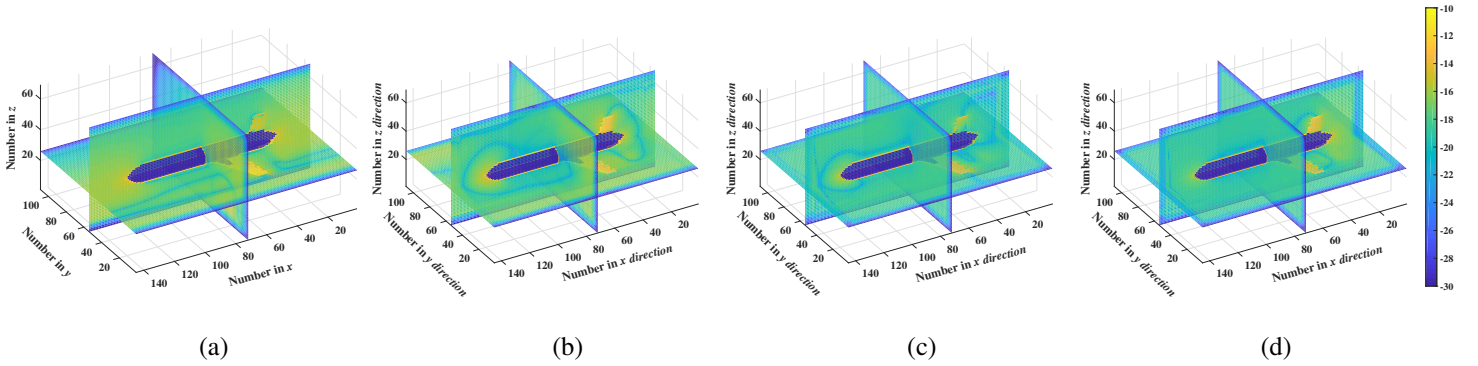


Fig. 17. The $\log(|E_x|)$ obtained by the CLOD-FDTD method with coarse meshes: (a) at $30ns$, (b) at $60ns$, (c) at $90ns$, (d) at $120ns$.

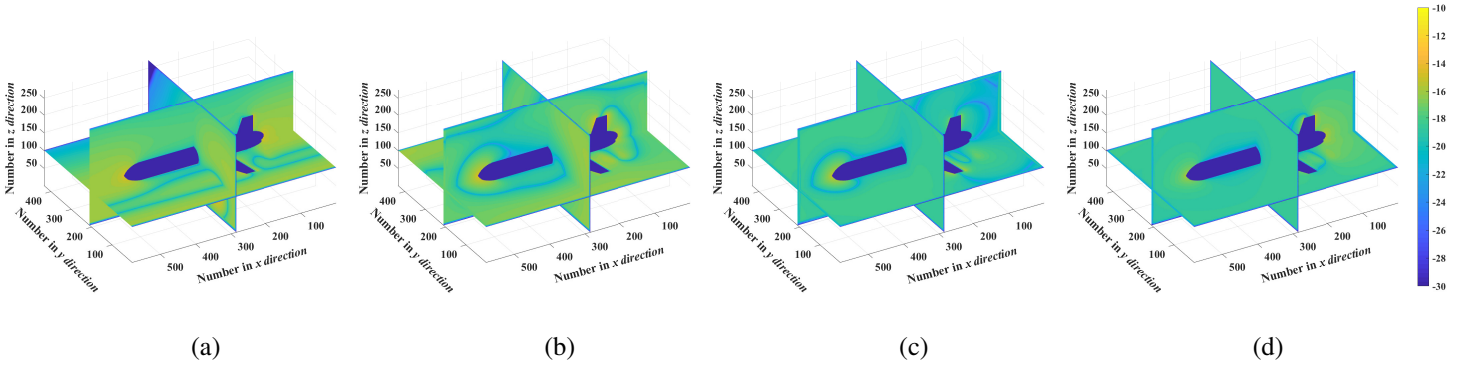


Fig. 18. The $\log(|E_x|)$ obtained by the LOD-FDTD method with fine meshes: (a) at $30ns$, (b) at $60ns$, (c) at $90ns$, (d) at $120ns$.

that, the result in the CLOD-FDTD method agrees well with the results obtained from the LOD-FDTD method with fine meshes. Therefore, the proposed CLOD-FDTD method can indeed improve the accuracy with coarse meshes.

Table II shows the overall number of cells and time cost for the LOD-FDTD method and the CLOD-FDTD method. It can be found from Table II that for the conventional LOD-FDTD method, the overall number of cells is 68,152,320 in fine meshes, which is 64 times that in coarse meshes. Besides, Δt used in the simulations with fine meshes is only a quarter of time steps for coarse meshes with the same CFLN. Therefore, CPU time of the LOD-FDTD method with fine meshes is at least 256 times that for coarse meshes. However, due to the significant increase of CPU time in memory access for large-

scale data set, the practical CPU time of the LOD-FDTD method with fine meshes is more than 360 times that for coarse meshes. By increasing CFLN to 4, the time cost for the LOD-FDTD method with coarse meshes can be reduced to 33,700.6s, which obtain a $5.2\times$ efficiency gain. However, the overall time cost is still much longer than that with coarse meshes.

On the other hand, the CLOD-FDTD method with coarse meshes takes 691.4s and 173.3s to complete the simulation when CFLN = 1, 4, relatively. Since additional modifications are required to be made in (2a)-(2f) and (3a)-(3f), it is slightly slower than the LOD-FDTD method with the same meshes. However, previous results have confirmed that the accuracy of the proposed CLOD-FDTD method with coarse meshes is

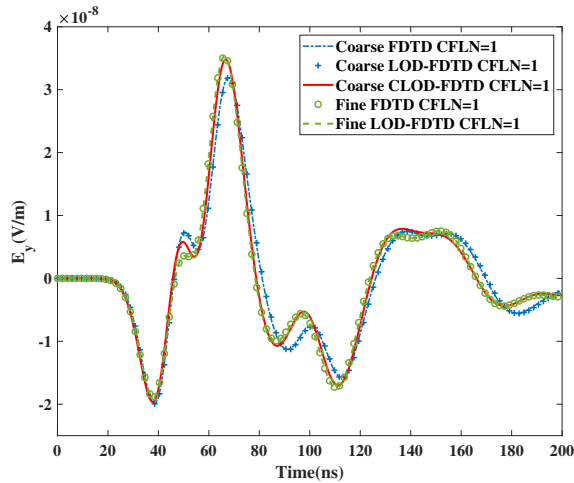


Fig. 19. E_y obtained from the FDTD method, the LOD-FDTD method and the proposed CLOD-FDTD method from $0ns$ to $200ns$ with CFLN = 1.

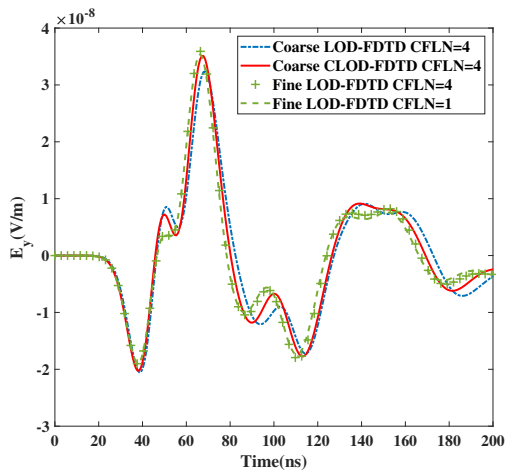


Fig. 20. E_y obtained from the LOD-FDTD method and the proposed CLOD-FDTD method from $0ns$ to $200ns$ with CFLN = 1, 4.

almost the same as those obtained by the LOD-FDTD method with fine meshes, which implies that less CPU time can be used in the proposed CLOD-FDTD method without sacrificing its accuracy by using coarse meshes. As shown in Table II, the speed-up ratio of the proposed CLOD-FDTD method with coarse meshes can be up to 255.3 and 1018.4 when CFLN = 1, 4, respectively.

We used coarse meshes with cell size as $0.05m$ and fine meshes with cell size as $0.025m$. The probe and the excitation are placed at $(9, 3, 1.4)[m]$ and $(9, 2.5, 1.4)[m]$, respectively. Results obtained by the LOD-FDTD and the CLOD-FDTD method with CFLNs = 1, 8 are shown in Fig. 21. It can be found that results with CFLN = 8 have slightly larger values and some delays because of the numerical dispersion error. However, results from the CLOD-FDTD method agree better with the reference results which obtained by the LOD-FDTD method with fine meshes.

Numerical results demonstrate that the CLOD-FDTD method is accurate in modeling curved surfaces with coarse

TABLE II
THE COMPUTATIONAL CONSUMPTION OF THE LOD-FDTD METHOD AND THE CLOD-FDTD METHOD WITH DIFFERENT CFLNS AND MESHES

Method		CFLN	Δt [ns]	No. of Cells	Time Cost [s]	Ratio*
LOD-FDTD	Coarse	1	0.193	1,064,880	490.1	360.1
		4	0.770	1,064,880	122.0	1446.6
		8	1.54	1,064,880	63.5	2779.3
	Fine	1	0.048	68,152,320	176,489.0	1.0
		4	0.193	68,152,320	33,700.6	5.2
		8	0.385	68,152,320	20550.7	8.5
CLOD-FDTD	Coarse	1	0.193	1,064,880	691.4	255.3
		4	0.770	1,064,880	173.3	1018.4
		8	1.54	1,064,880	90.7	1945.8
FDTD	Coarse	1	0.193	1,064,880	88.1	2003.3
	Fine	1	0.048	68,152,320	16685.2	10.58

* Ratio is defined as the ratio of time cost used in the LOD-FDTD method with fine meshes to that of the corresponding method.

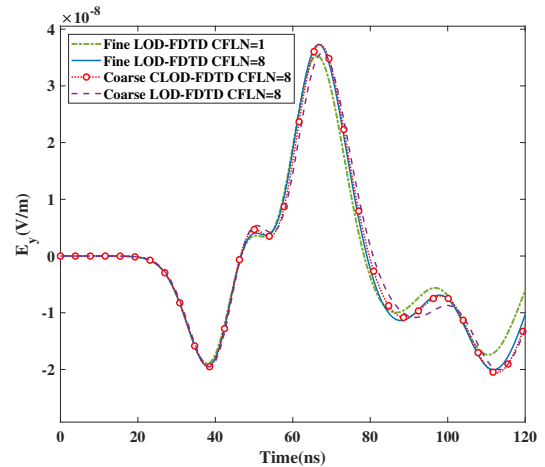


Fig. 21. E_y obtained from the LOD-FDTD method and the CLOD-FDTD method with CFLN = 1 and 8 from $0ns$ to $120ns$.

meshes. Therefore, significant performance improvement in terms of CPU time and memory consumption can be obtained.

V. CONCLUSION

In summary, we have proposed a three-dimensional CLOD-FDTD method to accurately model the curved PEC objects through carefully considering partially filled cells. Unlike other existing CFDTD methods, which suffer from time step reduction to guarantee the stability when the PEC objects are involved, the proposed CLOD-FDTD method still preserves unconditional stability. Numerical results validate its accuracy and efficiency. Therefore, it can decrease staircase error without time step reduction, which implies that higher simulation efficiency can be obtained compared with the traditional LOD-FDTD method. It shows quite promising potential in solving the EMC problems.

REFERENCES

[1] K. S. Yee, "Numerical solution of initial boundary value problems involving Maxwell's equations in isotropic media", *IEEE Trans. Antennas Propag.*, Vol. AP-14, No. 3, pp. 302-307, May 1966.

- [2] A. Taflove and S. C. Hagness, *Computational Electrodynamics: The Finite-Difference Time-Domain Method*, Norwood, MA, USA: Artech House, 2005.
- [3] A. G. Taflove, A. Oskooi, and S. G. Johnson, *Advances in FDTD Computational Electrodynamics: Photonics and Nanotechnology*, Norwood, MA, USA: Artech House, 2013.
- [4] T. Namiki, "A new FDTD algorithm based on alternating-direction implicit method," *IEEE Trans. Microw. Theory Techn.*, vol. 47, no. 10, pp. 2003-2007, Oct. 1999.
- [5] F. Zheng, Z. Chen, and J. Zhang, "Toward the development of a three-dimensional unconditionally stable finite-difference time-domain method," *IEEE Trans. Microw. Theory Techn.*, vol. 48, no. 9, pp. 1550-1558, Sept. 2000.
- [6] J. Shibayama, M. Muraki, J. Yamauchi, and H. Nakano, "Efficient implicit FDTD algorithm based on locally one-dimensional scheme," *Electron. Lett.*, vol. 41, no. 19, pp. 1046-1047, Sept. 2005.
- [7] I. Ahmed, E. Chua, E. Li, and Z. Chen, "Development of the Three-Dimensional Unconditionally Stable LOD-FDTD Method," *IEEE Trans. Antennas Propag.*, vol. 56, no. 11, pp. 3596-3600, Nov. 2008.
- [8] Q. F. Liu, Z. Chen, and W. Y. Yin, "An Arbitrary-Order LOD-FDTD Method and its Stability and Numerical Dispersion," *IEEE Trans. Antennas Propag.*, vol. 57, no. 8, pp. 2409-2417, Aug. 2009.
- [9] G. Sun and C. W. Trueman, "Unconditionally-stable FDTD method based on Crank-Nicolson scheme for solving three-dimensional Maxwell equations," *Electron. Lett.*, vol. 40, no. 10, pp. 589-590, May, 2004.
- [10] G. Sun and C. W. Trueman, "Efficient implementations of the Crank-Nicolson scheme for the finite-difference time-domain method," *IEEE Trans. Microw. Theory Techn.*, vol. 54, no. 5, pp. 2275-2284, May 2006.
- [11] E. L. Tan, "Efficient Algorithms for Crank-Nicolson-Based Finite-Difference Time-Domain Methods," *IEEE Trans. Microw. Theory Techn.*, vol. 56, no. 2, pp. 408-413, Feb. 2008.
- [12] W. Fu and E. L. Tan, "Development of split-step FDTD method with higher-order spatial accuracy," *Electron. Lett.*, vol. 40, no. 20, pp. 1252-1253, Jun. 2004.
- [13] G. Singh, E. L. Tan, and Z. N. Chen, "A Split-Step FDTD Method for 3-D Maxwell's Equations in General Anisotropic Media," *IEEE Trans. Antennas Propag.*, vol. 58, no. 11, pp. 3647-3657, Nov. 2010.
- [14] A. Grande, J. é. A. Pereda, A. Serroukh, I. Barba, A. C. Cabeceira, and J. é. Represa, "Reinterpreting Four-Stage Split-Step FDTD Methods as Two-Stage Methods," *IEEE Trans. Antennas Propag.*, vol. 61, no. 11, pp. 5818-5821, Nov. 2013.
- [15] S. J. Cooke, M. Botton, T. M. Antonsen, and B. Levush, "A leapfrog formulation of the 3D ADI-FDTD algorithm", *Int. J. Numer. Model.*, vol. 22, no. 2, pp. 187-200, 2009.
- [16] S. C. Yang, Z. D. Chen, Y. Q. Yu, and W. Y. Yin, "The Unconditionally Stable One-Step Leapfrog ADI-FDTD Method and Its Comparisons With Other FDTD Methods," *IEEE Microw. Wireless Compon. Lett.*, vol. 21, no. 12, pp. 640-642, Dec. 2011.
- [17] S. C. Yang, Z. D. Chen, Y. Q. Yu, and W. Y. Yin, "An Unconditionally Stable One-Step Arbitrary-Order Leapfrog ADI-FDTD Method and Its Numerical Properties," *IEEE Trans. Antennas Propag.*, vol. 60, no. 4, pp. 1995-2003, Apr. 2012.
- [18] Y. D. Kong and Q. X. Chu, "An unconditionally-stable FDTD method based on split-step scheme for solving three-dimensional maxwell equations," *IEEE International Conference on Microwave and Millimeter Wave Technology, 2008*, Nanjing, China, vol. 1, pp. 194-197, Apr. 2008.
- [19] N. Kaneda, B. Houshm, and T. Itoh, "FDTD analysis of dielectric resonators with curved surfaces," *IEEE Trans. Microw. Theory Techn.*, vol. 45, no. 9, pp. 1645-1649, Sept. 1997.
- [20] J. Wang, W. Y. Yin, P. G. Liu, and Q. H. Liu, "High-Order Interface Treatment Techniques for Modeling Curved Dielectric Objects," *IEEE Trans. Antennas Propag.*, vol. 58, no. 9, pp. 2946-2953, Sept. 2010.
- [21] S. Dey and R. Mittra, "A conformal finite-difference time-domain technique for modeling cylindrical dielectric resonators," *IEEE Trans. Microw. Theory Techn.*, vol. 47, no. 9, pp. 1737-1739, Sept. 1999.
- [22] J. Wang and W. Y. Yin, "Development of a novel FDTD (2, 4) compatible conformal schemes for electromagnetic computations of complex curved PEC objects," *IEEE Trans. Antennas Propag.*, vol. 61, no. 3, pp. 299-309, Jan. 2013.
- [23] I. A. Zagorodnov, R. Schuhmann, and T. Weiland, "A uniformly stable conformal FDTD-method in cartesian grids," *Int. J. Numer. Model.*, vol. 16, no. 2, pp. 127-141, Mar. 2003.
- [24] T. Xiao and Q. H. Liu, "Enlarged cells for the conformal FDTD method to avoid the time step reduction," *IEEE Microw. Wireless Compon. Lett.*, vol. 14, no. 12, pp. 551-553, Dec. 2004.
- [25] M. Chai, T. Xiao, and Q. H. Liu, "Conformal method to eliminate the ADI-FDTD staircasing errors," *IEEE Trans. Electromagn. Compat.*, vol. 48, no. 2, pp. 273-281, May 2006.
- [26] J. Dai, Z. Chen, D. Su, and X. Zhao, "Stability analysis and improvement of the conformal ADI-FDTD methods," *IEEE Trans. Antennas Propag.*, vol. 59, no. 6, pp. 2248-2258, Jun. 2011.
- [27] X. Wei, W. Shao, S. Shi, Y. Zhang, and B. Wang, "An efficient locally one-dimensional finite-difference time-domain method based on the conformal scheme," *Chin. Phys. B*, vol. 24, no. 7, pp. 76-84, May 2015.
- [28] H. Liu, X. Zhao, X. Wang, S. Yang, and Z. Chen, "Three-Dimensional Conformal LOD-FDTD Method for Accurate Transient Electromagnetic Analysis," *Int. Appl. Comput. Electromagn. Soc. Symp.-China (ACES)*, Chengdu, 2020.
- [29] J. Shibayama, M. Muraki, J. Yamauchi, and H. Nakano, "Efficient implicit FDTD algorithm based on locally one-dimensional scheme," *Electron. Lett.*, vol. 41, no. 19, pp. 1046-1047, Sept. 2005.
- [30] T. Su, Y. Liu, W. Yu, and R. Mittra, "A conformal mesh-generating technique for the conformal finite-difference time-domain (CFDTD) method," *IEEE Trans. Antennas Propag.*, vol. 46, no. 1, pp. 37-49, Feb. 2004.
- [31] G. Waldschmidt and A. Taflove, "Three-dimensional CAD-based mesh Generator for the Dey-Mittra conformal FDTD algorithm," *IEEE Trans. Antennas Propag.*, vol. 52, no. 7, pp. 1658-1664, Jul. 2004.
- [32] M. K. Berens, I. D. Flintoft, and J. F. Dawson, "Structured Mesh Generation: Open-source automatic nonuniform mesh generation for FDTD simulation," *IEEE Trans. Antennas Propag.*, vol. 58, no. 3, pp. 45-55, Jun. 2016.
- [33] X. C. Bo, X. Jin, J. F. Zhang, and C. T. Jun, "Study of Corner Singularity in Conformal Structured Mesh Generation for the Finite-Difference Time-Domain Method Based on Ray Tracing," *IEEE Trans. Microw. Theory Techn.*, vol. 67, no. 1, pp. 57-69, Jan. 2019.
- [34] T. Sauer, *Numerical Analysis*, 2nd ed. New York, NY, USA: Pearson, 2005.
- [35] Q. F. Liu, Z. Chen, and W. Y. Yin, "An arbitrary-order LOD-FDTD method and its stability and numerical dispersion," *IEEE Trans. Antennas Propag.*, vol. 57, no. 8, pp. 2409-2417, Aug. 2009.
- [36] S. Dey and R. Mittra, "A locally conformal finite-difference time-domain (FDTD) algorithm for modeling three-dimensional perfectly conducting objects," *IEEE Microw. Guided. W.*, vol. 7, no. 9, pp. 273-275, Sept. 1997.
- [37] S. Yang, Z. Chen, Y. Yu, and S. Ponomarenko, "Efficient Implementation of the Divergence-Preserved ADI-FDTD Method," *IEEE Antennas Wireless Propag. Lett.*, vol. 11, pp. 1560-1563, Dec. 2012.
- [38] F. Zheng and Z. Chen, "Numerical dispersion analysis of the unconditionally stable 3-D ADI-FDTD method," *IEEE Trans. Microw. Theory Techn.*, vol. 49, no. 5, pp. 1006-1009, May 2001.
- [39] J. Pereda, O. Garcia, A. Vegas, and A. Prieto, "Numerical dispersion and stability analysis of the FDTD technique in lossy dielectrics," *IEEE Microwave Guided Wave Lett.*, vol. 8, no. 7, pp. 245-247, Jul. 1998.
- [40] I. Ahmed, E. Chua, and E. Li, "Numerical Dispersion Analysis of the Unconditionally Stable Three-Dimensional LOD-FDTD Method," *IEEE Trans. Antennas Propag.*, vol. 58, no. 12, pp. 3983-3989, Dec. 2010.
- [41] J. A. Roden and S. D. Gedney, "Convolutional PML (CPML): An efficient FDTD implementation of the CFS-PML for arbitrary media," *Microw. Opt. Technol. Lett.*, vol. 27, pp. 334-339, 2000.
- [42] I. Ahmed, E. Li, and K. Krohne, "Convolutional Perfectly Matched Layer for an Unconditionally Stable LOD-FDTD Method," *IEEE Microw. Wireless Compon. Lett.*, vol. 17, no. 12, pp. 816-818, Dec. 2007.